AD-A115 061 ALUMINUM CO OF AMERICA ALCOA CENTER PA ALCOA LABS F/G 11/6
EVALUATION OF THE ENGINEERING PROPERTIES OF A COMMERCIALLY PROD--ETC(U)
DEC 81 R C MALCOLM, A VASUDEVAN, R J BUCCI N00019-79-C-0258

UNCLASSIFIED NL

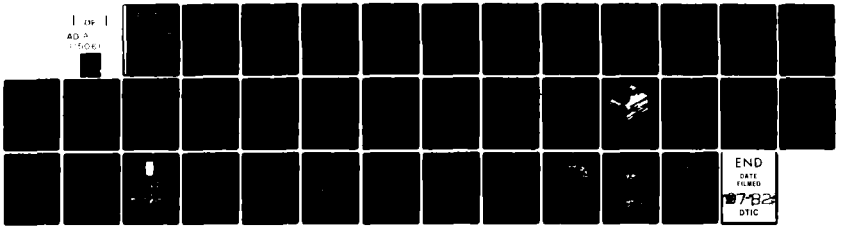

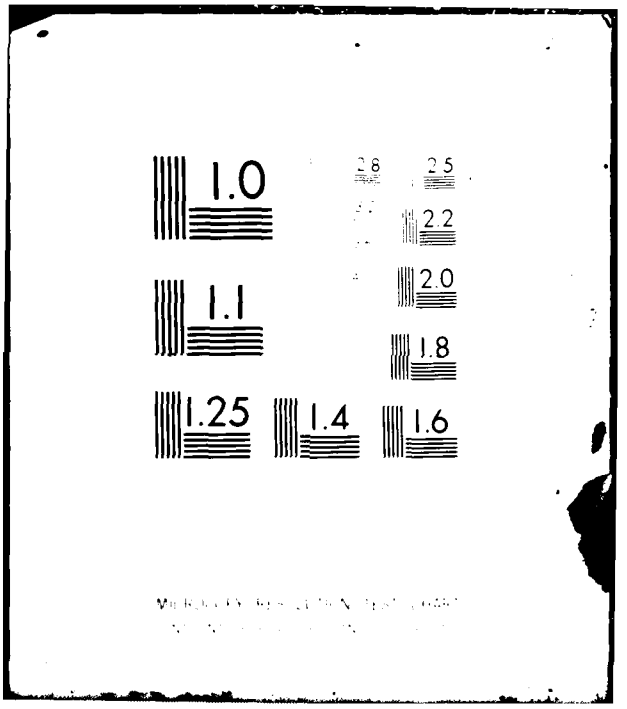
1.0
2.8
2.5
2.2
1.1
2.0
1.8
1.25
1.4
1.6

Evaluation of the Engineering Properties of A Commercially Produced Aluminum Alloy 2020-T651 Plate

R.C. Malcolm
A.K. Vasudevan
R.J. Bucci
P.E. Bretz
Aluminum Company of America

Report Submitted to Fulfill Agreement Under Amendment to Contract N00019-78-C-0256

Prepared for
Department of the Navy
Naval Air Systems Command
Washington, D.C. 20360

[illegible] December 19

ALCOA

TABLE OF CONTENTS

UNCLASSIFIED

SECURITY CLASSIFICATION OF THIS PAGE (When Data Entered)

REPORT DOCUMENTATION PAGE		READ INSTRUCTIONS BEFORE COMPLETING FORM
1. REPORT NUMBER	2. GOVT ACCESSION NO. AD-A115 631	3. RECIPIENT'S CATALOG NUMBER
4. TITLE (and Subtitle) Evaluation of the Engineering Properties of a Commercially Produced Aluminum Alloy 2020-T651 Plate		5. TYPE OF REPORT & PERIOD COVERED Final 6. PERFORMING ORG. REPORT NUMBER
7. AUTHOR(s) R. C. Malcolm, A. K. Vasudevan, R. J. Bucci, F. E. Heuer		8. CONTRACT OR GRANT NUMBER(s) Amendment [illegible] N00019-[illegible]
9. PERFORMING ORGANIZATION NAME AND ADDRESS Aluminum Company of America Alcoa Laboratories Alcoa Center, PA 15069		10. PROGRAM ELEMENT, PROJECT, TASK AREA & WORK UNIT NUMBERS
11. CONTROLLING OFFICE NAME AND ADDRESS Department of the Navy Naval Air Systems Command Washington, DC 20361		12. REPORT DATE 1981 December 18 13. NUMBER OF PAGES
14. MONITORING AGENCY NAME & ADDRESS (if different from Controlling Office)		15. SECURITY CLASS. (of this report) Unclassified 15a. DECLASSIFICATION/DOWNGRADING SCHEDULE

16. DISTRIBUTION STATEMENT (of this Report)

APPROVED FOR PUBLIC RELEASE; DISTRIBUTION UNLIMITED

17. DISTRIBUTION STATEMENT (of the abstract entered in Block 20, if different from Report)

18. SUPPLEMENTARY NOTES

19. KEY WORDS (Continue on reverse side if necessary and identify by block number)

Aluminum Alloy	Tensile Properties	
Aluminum-Lithium Alloy	Tear Properties	Resistance R-Curves
2020-T651	Fatigue Crack Growth	Slow Bend Charpy
Chemical Analysis	Fracture Toughness	Fractography
Mechanical Properties	K_{Ic}	

20. ABSTRACT (Continue on reverse side if necessary and identify by block number)

Al-Cu-Li alloy 2020 was developed in the 1950's to help satisfy the need for high strength and high modulus of elasticity in an aircraft structural material. The fracture toughness of alloy 2020 is comparatively low compared to other aerospace alloys. This characteristic coupled with manufacturing difficulty eventually led to the withdrawal of alloy 2020 for use in commercial products. Despite this setback, aluminum alloys containing lithium remain attractive for aircraft applications because in addition to high strength

DD FORM 1 JAN 73 1473 EDITION OF 1 NOV 65 IS OBSOLETE

UNCLASSIFIED

SECURITY CLASSIFICATION OF THIS PAGE (When Data Entered)

and high elastic modulus, they possess low density and the potential for higher resistance to fatigue. Consequently, current research has been directed toward increasing fracture toughness of Al-Li type alloys into a range acceptable for aircraft use.

This report summarizes tensile, fracture toughness and fatigue crack growth properties obtained from a commercially produced lot of aluminum alloy 2020-T651 plate. This characterization is intended to serve as a baseline for alloy development work directed at improving damage tolerant characteristics of Al-Li type alloys. The fracture toughness characterization includes plane-strain fracture toughness (K_{Ic}) values, crack growth resistance (R) curves, as well as results from fracture toughness indicator tests; namely, the Kahn-type tear test and the slow bend precrack charpy test. Obtained fatigue crack growth rates traverse the entire range from near-threshold values to the exceedingly high rates encountered as ΔK values approach the material toughness. Metallographic characterization of alloy 2020-T651 in addition to fractographic results from a fatigue crack growth test specimen are also included in this report.

FOREWORD

To assist studies in the area of aluminum-lithium alloy development, Alcoa requested the Navy supply samples of commercially produced 2020-T651 plate for the purpose of developing baseline engineering data. In exchange for two pieces of 2020-T651 plate from the Navy's inventory, Alcoa agreed to characterize the plate and submit the test results at no cost to the Navy. This transaction was handled as an amendment to Navy Contract No. N00019-79-C-0258 which was concurrently under way during the period 1979 July 1 to 1981 June 30 at Alcoa Laboratories, Alcoa Center, Pennsylvania. Mr. M. D. Valentine was the Navy Contract Monitor. R. J. Bucci served as Alcoa project manager, with R. C. Malcolm, A. K. Vasudevan, and P. E. Bretz as the principal Alcoa engineer/scientists for the program. A selected fatigue crack growth test was subcontracted to Del Research Corporation, Hellertown, Pennsylvania, under the direction of J. K. Donald and G. Miller as principal engineer.

LIST OF TABLES

LIST OF FIGURES

LIST OF FIGURES (continued)

EVALUATION OF THE ENGINEERING PROPERTIES OF A COMMERCIALLY PRODUCED ALUMINUM ALLOY 2020-T651 PLATE

INTRODUCTION

Aluminum alloy 2020, which has a nominal composition of 4.5% Copper, 1.1% Lithium, 0.5% Manganese, 0.5% Cadmium and the balance Aluminum (93.7%), was developed in the 1950's to help satisfy the need for alloys with high strength and high modulus of elasticity for use in aircraft structures. However, alloy 2020, particularly in the peak strength temper (T6), developed low fracture toughness compared to that of commercial 7XXX alloys. This characteristic coupled with manufacturing difficulty led to the withdrawal of alloy 2020 for use in commercial products. Despite this setback, aluminum alloys containing lithium remain attractive for aircraft applications because in addition to high strength and high modulus of elasticity, they possess low density and the potential for higher resistance to cyclic loading conditions.(1, 2) Consequently, current research has been directed toward increasing fracture toughness of Al-Li-type alloys into a range acceptable for aircraft use.(2, 3)

To aid studies in the area of Al-Li-type alloy improvement, Alcoa requested the Navy supply some 2020-T651 plate for the purpose of developing engineering characteristics of alloy 2020 as a baseline material. In exchange for two pieces of aluminum alloy 2020-T651 plate (fabricated from the same lot) supplied by the Naval Air Systems Command, Alcoa agreed to characterize the plate and submit the test results and evaluations at no additional cost to the Navy. This transaction (4) was handled as an amendment to Navy Contract No. N00019-79-C-0258, "Effect of Microstructure on 7XXX Aluminum Alloy Fatigue Crack Growth at Low Stress Intensity."

OBJECTIVES

The properties agreed upon to be evaluated on the 2020-T651 plate are as follows:

1. Characterize microstructure by light microscopy,
2. chemical analysis,
3. tensile,
4. tear,
5. fracture toughness,
6. fatigue crack growth in humid air at room temperature (low, intermediate, and high ΔK), and
7. fractography.

MATERIAL

Two pieces of a single lot of commercially produced 32.54 mm (1.281-in.) thick 2020-T651 plate was supplied by the Navy for testing and study. Both pieces of plate were identical in size and shape, as shown in Fig. 1. Also, as indicated in Fig. 1, the rolling direction (longitudinal) of each piece of plate is parallel to the longest dimension (4.44 m or 14 ft. 7 in.). An Alcoa Technical Center sample number (523713) was assigned to each piece of plate with one denoted "A" and the other "B". A typical optical micrograph of the alloy is shown in Fig. 2. The structure is composed of coarse recrystallized grains. The grain size along longitudinal direction is ~380 μm.

The chemical composition of each piece of plate was determined and the remelt analysis of each is shown in Table 1.

SPECIMENS AND TEST PROCEDURES

Test specimens to determine the various mechanical properties of both pieces of 2020-T651 plate were taken from Section 2 location in each piece, as shown in Fig. 1. The location of each individual specimen taken from Section 2 of pieces "A" and "B" is shown in Figs. 3 and 4, respectively. All the mechanical properties were determined from tests at room temperature on specimens taken in both the longitudinal and long-transverse orientations with respect to the rolling direction of each piece of plate.

1. Tensile Tests

The tensile tests were conducted in accordance with the ASTM Standard Method B557 using nominally 12.7 mm (0.500-in.) diameter specimens. Tests were made of both plate pieces "A" and "B" and in both the longitudinal (L) and long-transverse (LT) directions.

2. Tear Tests

The tear tests were made using nominally 2.54 mm (0.100-in.) thick Kahn-type tear test specimens. Tests were made of both plate pieces "A" and "B" and in both the longitudinal (L-T) and long-transverse (T-L) orientations.

The energy required to initiate and propagate a crack in each specimen were both determined from measurements of the appropriate areas under autographic load-deformation curves of the types represented in Fig. 5. The unit-propagation energy, which is used as an index of tear resistance, was determined for each specimen by dividing the net area of the specimen into the energy to propagate the crack. The ratio of the tear strength (the maximum nominal combined direct-and-bending stress developed by the specimen) to the tensile-yield strength was determined for each specimen for use as an index of toughness.

3. Fracture Toughness Tests

A. K_{Ic}

The fracture toughness K_{Ic} tests were conducted in accordance with the ASTM Standard Method E399 using nominally 31.8 mm (1.250-in.) thick compact-tension fracture toughness specimens, W = 63.5 mm (2.500-in.) and 2H = 76.2 mm (3.000-in.).

Tests were made of both 7075-T651 plate pieces "A" and "B" and in both the longitudinal (L-T) and long-transverse (T-L) orientations.

B. R-Curve

R-curve tests to determine material toughness were conducted in accordance with ASTM Standard Method E561 using nominally 7.35 mm (0.29-in.) thickness compact fracture mechanics specimens of the geometry shown in Fig. 1. Tests were made on specimens taken only from plate piece "B" and in both the L-T and T-L orientations.

Each specimen was fatigue precracked to a crack length about five percent greater than that corresponding to the initial machined notch. All specimens were loaded to failure at a controlled rate of displacement of 0.64 mm (0.1-in.) per minute at the load points. During the loading, crack opening displacement (COD) values were measured by a clip-on displacement gage mounted at the crack mouth. The R-curve was developed by defining a series of secant offset lines emanating from the origin (zero load point) and intersecting the autographic load-COD trace. The slope defined by the secant offset defines an effective elastic compliance, which can be correlated to an effective crack length (a_{eff}) through the specimen compliance relationship. The a_{eff} value represents the sum of the initial crack length (a_o) and the incremental effective crack extension (Δa_{eff}), the latter being the sum of the actual crack growth (Δa) and the crack tip plastic zone adjustment at the applied load. The K_R values are calculated using a_{eff} and the load at the secant intersection of the load vs. COD trace as input parameters to the stress intensity factor expression for the compact specimen.

C. Slow Bend Charpy

Slow bend Charpy (SBC) tests, used as an alloy fracture toughness indicator, were made using specimens of the configuration shown in Fig. 7. Tests were made on specimens taken only from plate piece "B" and in both the L-T and T-L orientations. Two SBC specimen thicknesses, 8.35 mm (0.329-in.) and the standard 10 mm (0.395-in.), were tested. The SBC specimens were fatigue precracked in simple bending to a nominal 5.18 mm (0.139-in.) length beyond the machined notch tip. Each specimen was then loaded to failure as a simply supported beam, as shown in Fig. 8, with deflection of the beam under load measured by two linear variable differential transformers (LVDT's). The electronic load and displacement signals were processed by computer and plotted as indicated in Fig. 9. One of the curves shown in the figure represents the total energy absorbed by the specimen and is calculated as the area under the load-deformation diagram.

Work by Ronald(5) and Wyponik(6) conducted on high strength titanium and aluminum alloys respectively, showed good correlation between K_{Ic} and SBC (K_{Ich}) toughness values calculated according to the following expression:

$$K_{Ich} = \left[\frac{E\,(\overline{W}/A)}{3\,(1-\mu)} \right]^{\frac{1}{2}}$$

Where: E = modulus of elasticity

$\overline{W}$ = total work done fracturing the specimen given by the plateau value of the energy curve, see Fig. 4

A = gross original area of the uncracked specimen ligament

μ = Poisson's ratio = 0.33.

c. Fatigue-Crack-Growth-Rate Tests

Constant-load-amplitude fatigue crack growth (FCG) tests were conducted over the low, intermediate and high stress intensity (ΔK) range on specimens from the plate "B" of the 7075-T651 plate. Crack-growth rate data was obtained using the standard ASTM E-647 compact-tension (CT) specimen, B = 4.19 mm (0.165 in.) and W = 50.8 mm (2.0 in.), in the L-T and T-L orientations. Three FCG tests were made, two at the Alcoa Technical Center (one test of each orientation), and one at Del Research, Hollister, CA (using an L-T oriented specimen). All the testing was performed on MTS servo-controlled (programmable-digital-function-generator) closed-loop mechanical test machines at a stress ratio (R = K_{min}/K_{max} equal to 0.05) and a test frequency of 25 Hertz. The test environment was high humidity (relative humidity > 90%)-room temperature-laboratory air.

The precracking of the specimens tested at the Alcoa Technical Center was conducted by a schedule of stepped-load reductions (R-ratio = 0.05, frequency = 25 Hz) with increasing crack extension. Upon attaining the desired value of ΔK, the precrack phase was terminated and then FCG rate measurements were made at ΔK increased with crack extension under fixed amplitude loading. The method of crack growth measurement was visual.

The precracking of the specimen tested at Del Research was conducted at an R-ratio of 0.1 with visual crack growth measurement. Upon attaining the desired crack length, a, the test parameters were applied. An automated test system utilizing a computer for data acquisition and machine control was used to obtain the crack growth rate data. The crack length was monitored continuously by using the elastic compliance technique, enabling the stress intensity to be controlled according to the equation:

$$K = K_0 \exp\left[\gamma (a-a_0)\right]$$

(K_0 is the initial cyclic stress intensity corresponding to the initial crack length, a_0; "a" is the current crack length, and γ is a constant with the dimensions of 1/length(7)). The test (K-decreasing) was conducted using a value of $-36.1\ mm^{-1}$ ($-1.5\ in.^{-1}$) for the parameter γ. Also, for comparison, a couple of crack length measurements were made visually during the test.

The test procedures strictly adhered to the ASTM Tentative Test Method for Constant-Load-Amplitude Fatigue Crack Growth Rates Above 10^{-8} m/cycle, E-647, and the proposed ASTM Standard test practice for measurement of very slow fatigue crack rates ($da/dN < 10^{-8}$ m/cycle)(8).

MECHANICAL PROPERTIES

1. Tensile

The results of the tensile tests of both pieces (A and B) of 2020-T651 plate in the L and LT directions are shown in Table 2. Duplicate tests were conducted for each condition, with the exception that four tests were made of piece "A" in the LT direction.

In general, the tensile properties of plate pieces "A" and "B" are comparable. Also, the tensile and yield strengths of each plate in the L and LT directions are comparable. However, the elongation and reduction of area values for both pieces of plate in the L direction are significantly higher than corresponding LT direction values.

2. Tear

The results of the tear tests of both pieces (A and B) of 2020-T651 plate in the L-T and T-L orientations are shown in Table 3. Duplicate tests were conducted for each condition.

In general, the tear strengths, ratios of tear strength to tensile-yield strength, and unit propagation energy values shown in Table 3 for both pieces of plate (A and B) are quite low, therefore, indicating that the fracture toughness of the 2020-T651 plate may not be very high. However, in general, the properties are comparable to those of another sample of Alcoa produced 34.9 mm (1.375-in.) thick 2020-T651 plate tested previously (unpublished Alcoa data).

The tear properties of plate piece "A" are slightly higher than those of piece "B". All of the L-T oriented tear specimens from both plate pieces fractured diagonally, as shown in Fig. 1C, whereas the fracture path of each of the T-L oriented specimens is normal. The tear properties in the L-T orientation of both pieces of plate are significantly higher than these properties in the T-L orientation.

3. Fracture Toughness

A. K_{Ic}

The results of the K_{Ic} tests of told pieces (A and B) of 2020-T651 plate in the L-T and T-L orientations are shown in Table 4. Duplicate tests were conducted for each condition.

The tests on specimens in the L-T orientation of both pieces of plate resulted in valid K_{Ic} values, however, none of the tests in the T-L orientation resulted in valid K_{Ic} values. On the other hand, the K_Q values for the T-L orientation of both plate "A" tests and one plate "B" test are considered meaningful. These test results show that the fracture toughness of plate pieces "A" and "B" are equal, however, the values are rather low indicating poor toughness. In general, the properties are comparable to those of two samples of Alcoa commercially produced 34.9 mm (1.375-in.) thick 2020-T651 plate tested previously (unpublished Alcoa data).

B. R-Curves

R-curves were developed from tests of specimens taken in the L-T and T-L orientations and only from plate piece "B". The data are shown in Fig. 6. Each curve is composed of data established from duplicate tests which were very reproducible. Out of plane fractures occurred in both the L-T oriented specimens, however not with the T-L oriented specimens. The data points recorded in Fig. 6 represent only those values where the plane of crack growth remained normal (to within $\pm 5°$) to the applied loading direction. For the higher toughness L-T orientation, out of plane fractures occurred at Δa_{eff} values which correspond approximately to the point of maximum test load.

C. Slow Bend Charpy

Slow bend charpy (CB``) tests were conducted on specimens taken in the L-T and T-L orientations and only from plate piece "B". Four tests were made on specimens in each orientation, two each of 10 mm (0.395-in.) and 6.35 mm (0.250-in.) thick specimens. The results of these tests are shown in Table [illegible].

The $K_{Q_{CB}}$ values determined from the 6.35 mm (0.250-in.) thick specimens are higher (on the average about 12 percent in the L-T orientation and [illegible] percent in the T-L orientation) than those values determined from the standard 10 mm (0.395-in.) thick specimens. The $K_{Q_{CB}}$ values shown in Table [illegible] for the L-T oriented specimens are significantly higher than those for the T-L oriented specimens. Also, the fracture path observed in all the CB specimens tested (L-T and T-L orientations) retained their original plane, thereby eliminating the confounding effect of out of plane fracture on test interpretation.

The $K_{Q_{CB}}$ values are comparable to the K_Q values (Table 4).

4. Fatigue Crack Growth (da/dN)

Constant-load-amplitude fatigue crack growth (FCG) da/dN tests were made only on specimens from the 2020-T651 plate piece "B". Two tests were conducted on CT specimens in the L-T orientation and one in the T-L orientation at an R-ratio of 0.33 in a moist-air environment. Crack growth measurements for two of the tests (specimen number 1 in the L-T orientation and number 1 in the T-L orientation) were determined visually and those for one test (specimen number 2 in the L-T orientation) were determined electronically (compliance method). The crack growth rate data, at low, intermediate and high stress intensities (ΔK) for the three tests are shown plotted together in Fig. 11.

Some of the data shown in Fig. 11 violate an ASTM E647 requirement that at a given number of cycles any two crack lengths differing by more than 0.25B, actually 1.57 mm (0.062-in.) for these two tests, is invalid. However, since the requirement is not violated by much, not more than 0.84 mm (0.033-in.) in any instance, and a significant amount of critical low ΔK data is involved, this data is included in Fig. 11 (represented by solid symbols). This decision is also substantiated by the fact that there is sufficient data that does not violate the requirement that is interspersed with the invalid data and is in good agreement indicating that the slight violation of the ASTM requirement can be tolerated in this instance.

For the given test conditions, specimens oriented in L-T or T-L show little or no difference in crack growth rate over the [illegible] MPa$\sqrt{m}$ ([illegible] ksi$\sqrt{in.}$) range of ΔK. However, [illegible] higher [illegible] the crack growth rates are generally faster in the T-L orientation than [illegible] in the L-T.

A comparison of the constant-amplitude [illegible] rate data determined using visual versus compliance methods of crack growth measurements on L-T oriented specimens is shown in Fig. [illegible]. Although the data determined using the compliance crack measurement method appear to possess generally slightly faster rates than the data determined by visual crack measurements, it is considered that the data are in good agreement. Since both crack measurement methods were [illegible] applied to each specimen, these differences are considered to be attributable to normal scatter.

A comparison of the [illegible] rate data for the [illegible]-T[illegible] plate in the L-T orientation, characterized in this report, with similar data for a sample of another Alcoa produced lot of [illegible]-T[illegible] plate, [illegible] mm (1.[illegible]-in.) thickness, tested previously [illegible] is shown in Fig. [illegible]. These data are comparable at the low, intermediate and high growth rates.

Comparison of the [illegible] rate data for the [illegible]-T[illegible] plate in the L-T orientation, with similar data for commercially and laboratory produced [illegible]-T[illegible] plate and commercially produced [illegible]-T[illegible] plate, tested previously [illegible], is shown in Fig. [illegible]. The [illegible] data representing each temper of [illegible] plate are shown as bands. The band for [illegible]-T[illegible] represents the test results of [illegible] plates, two of [illegible] commercially and [illegible] laboratory produced [illegible] mm ([illegible]-in.) in thickness [illegible] commercially produced [illegible] mm ([illegible]-in.) in thickness. The band for [illegible]-T[illegible] represents the test results of two lots of plate, one [illegible] mm ([illegible]-in.) in thickness and the other [illegible] mm ([illegible]-in.) in thickness. At low, intermediate and high [illegible] rates the [illegible]-T[illegible] plate generally exhibits superior resistance to crack growth under the same conditions [illegible] than the [illegible]-T[illegible]51 or [illegible]-T[illegible]51 plate.

5. Fractographic Evaluation

Figures 15a through 15f present the fatigue fracture topography of alloy [illegible]-T[illegible] plate (piece "[illegible]", [illegible], specimen [illegible]) in the L-T orientation, at crack growth rates from 1.[illegible] x $10^{-[illegible]}$ to 1.[illegible] x $10^{-[illegible]}$ m/cycle (5 x $10^{-[illegible]}$ to [illegible] x $10^{-[illegible]}$ in./cycle, respectively). For [illegible] rates up to 1.[illegible] x $10^{-[illegible]}$ m/cycle ([illegible] x $10^{-[illegible]}$ in./cycle), crack growth occurs primarily by a transgranular, crystallographic mechanism (Figs. 15a to 15d). [illegible] cracking is evident at 1.[illegible] x $10^{-[illegible]}$ and 1.[illegible] x $10^{-[illegible]}$ m/cycle ([illegible] x $10^{-[illegible]}$ and [illegible] x $10^{-[illegible]}$ in./cycle, respectively), as denoted by the letter C in Figs. 15c and 15d. A transition in fracture mechanism occurs at growth rates of 1.[illegible] x $10^{-[illegible]}$ and 1.[illegible] x $10^{-[illegible]}$ m/cycle ([illegible] x $10^{-[illegible]}$ and [illegible] x 10^{-5} in./cycle, respectively), as shown in Figs. 15e and 15f, respectively, to a mixed mode, dimpled rupture plus intergranular fracture path. Several specific fracture surface features are apparent at these higher growth rates, as shown in Figs. 15e and 15f, including fine-scale void formation (detail [illegible]), void nucleation at constituent particles (detail [illegible]), and intergranular fracture (detail [illegible]). This fracture topography in Figs. 15e and 15f is similar to that reported in a previous investigation [illegible] for the intermediate and high growth rate regimes.

SUMMARY

The chemical composition and various mechanical properties have been determined along with microstructural and fractographic examinations of a 32.54 mm (1.281-in.) thick sample of commercially produced 2020-T651 plate, two pieces (A and B), supplied by the Department of the Navy. The results of the various tests and examinations of the material are shown as follows:

1. Chemical Composition - Table 1

2. Microstructure Examination - Figure 2

3. Tensile Properties - Table 2

4. Tear Properties - Table 3

5. Fracture Toughness - Table 4 (K_{Ic} and Slow Bend Charpy) and Figure 6 (R-Curve)

6. Fatigue Crack Growth (FCG) - Figures 11 through 14

7. Fractographic Examination of FCG Specimen - Figure 15 (a-f)

The composition of the plate is about nominal for 2020 and the tensile properties of plate pieces "A" and "B" are comparable.

The fracture toughness of the plate is rather poor compared to 7XXX alloys and is indicated by the poor tear resistance and low K_{Ic}, R-curve and slow bend charpy values. On the other hand, the resistance of the 2020-T651 plate to constant-load-amplitude fatigue crack growth (FCG) at an R-ratio of 0.33 in a moist air environment is quite good over the low, intermediate and high ΔK ranges, and generally superior to 7075 plate in the T651 and T7351 tempers under similar conditions.

REFERENCES

1. T. H. Sanders and E. A. Starke, "Aluminum-Lithium Alloys: Low Density and High Strength," Metal Progress, March 1978, pp. 32-37.

2. T. H. Sanders and J. T. Staley, "Review of Fatigue and Fracture Resistance of High-Strength Aluminum Alloys," Fatigue and Microstructure, American Society of Metals, 1978, pp. 467-522.

3. T. H. Sanders, "Effects of Orientation on Fracture Toughness and Other Properties of Aluminum-Lithium Alloy," Final Report, Naval Air Development Center, Contract No. N62269-77-C-0471.

4. Letter from Harold J. Bridges, Manager of R&D Contracts, Alcoa Laboratories, to Dr. J. W. Schneider, Contracting Officer, Department of the Navy, Naval Air Systems Command, Washington, DC, Contract No. N00019-73-C-0356," 1978 January 24.

5. T. W. F. Russell, J. A. Hall, and D. M. Pierce, "Usefulness of Precracked Charpy Specimens for Fracture Toughness Screening Test of Titanium Alloys," Engineering Fracture Mechanics, Volume 5, April 1973, pp. 513-519.

6. R. J. Bucci, unpublished Alcoa data, 1978.

7. M. Saxena, J. J. Radak, Jr., C. E. Bennett, D. W. Schmidt, "Computer Controlled K-Decreasing Test Technique for Low Rate Fatigue Crack Growth Testing," J. Testing and Evaluation JTEVA, Volume 6, May 1978.

8. R. J. Bucci, "Development of a Proposed Standard Practice for Near-Threshold Fatigue Crack Growth Rate Measurement," ASTM STP 738, American Society for Testing and Materials, 1981, pp. 5-28.

TABLE 1

CHEMICAL COMPOSITION[a] OF TWO (2) PIECES[b] OF COMMERCIALLY PRODUCED 32.54 mm (1.281-in.) THICK ALUMINUM ALLOY 2020-T651 PLATE[c]

Plate Piece Identification	Element, %								
	Si	Fe	Cu	Mn	Zn	Ti	Li	Cd	Al
A	0.09	0.20	4.48	0.53	0.03	0.02	1.06	0.19	93.40
B	0.09	0.20	4.44	0.52	0.03	0.02	1.09	0.20	93.41
Average	0.09	0.20	4.46	0.52	0.03	0.02	1.08	0.20	93.40
Nominal	—	—	4.5	0.5	—	—	1.1	0.2	93.7

NOTES: (a) Remelt analysis.
(b) Fabricated from a single lot.
(c) Sample No. 523713 (Alcoa number).

TABLE 2

RESULTS OF TENSILE TESTS AT ROOM TEMPERATURE OF TWO (2) PIECES[a] OF COMMERCIALLY PRODUCED 32.54 mm (1.281-in.) THICK ALUMINUM ALLOY 2020-T651 PLATE[b]

Plate Piece Identification[c][d]	Specimen Orientation[e]	Specimen No.	TS[f] MPa	TS[f] KSI	YS[g] MPa	YS[g] KSI	El. in 4D,[h] %	R of A,[i] %
A	L	1[j]	545.5	79.1	516	74.8	5.8	9
		2	543.5	78.8	516	74.8	3.8	5
		Average	544.5	79.0	516	74.8	4.8	7
B	L	1[j]	550.5	79.8	519.5	75.3	5.8	9
		2[j]	550	79.8	519.5	75.3	5.8	8
		Average	550.2	79.8	519.5	75.3	5.8	8
A	LT	1[j][k]	521.5	75.6	516	74.8	0.9	2
		2[k]	480[l]	69.6[l]	(m)	(m)	0.9	0[l]
		3[k]	533.5	77.4	514	74.5	1.4	2
		4	520.5	75.5	514	74.5	0.4	2
		Average	525.2[n]	76.2[n]	514.7[n]	74.7[n]	0.9	2[n]
B	LT	1	541	78.5	521.5	75.6	1.4	2
		2[j][k]	538.5	78.1	521.5	75.6	1.4	1
		Average	539.8	78.3	521.5	75.6	1.4	2

NOTES:
(a) Fabricated from a single lot.
(b) Sample No. 523713 (Alcoa number).
(c) Specimens taken from Section 2 in each piece (refer to Fig. 1 for location of Section 2).
(d) Refer to Figs. 3 and 4 for location of test specimens in pieces A and B, respectively.
(e) Test specimens taken in the longitudinal (L) and long-transverse (LT) direction of rolling and from the center (T/2) location through the plate thickness.
(f) TS = Tensile Strength.
(g) YS = Yield Strength (0.2 percent offset).
(h) El. in 4D = Elongation in 4 times specimen diameter.
(i) R of A = Reduction of Area.
(j) Specimen fragmented at fracture.
(k) Specimen failed outside middle third of gage length.
(l) Value not included in the determination of average value.
(m) Value not obtained (specimen failed before reaching 0.2 percent offset).
(n) Value represents the average of three (3) tests.

TABLE 3

RESULTS OF TEAR TESTS AT ROOM TEMPERATURE OF TWO (2) PIECES[a] OF COMMERCIALLY PRODUCED 32.54 mm (1.281-in.) THICK ALUMINUM ALLOY 2020-T651 PLATE[b]

Plate Piece[c][d] Identification	Specimen Orientation[e]	Specimen No.	TS[f] MPa	TS[f] KSI	TS/YS[g] Ratio	UPE[h] KJ/m²	UPE[h] in.-lb/in.²
A	L-T	1	428	62.1	0.83	30.2[i][j]	172[i][j]
		2	451	65.4	0.87	28.6[i][j]	163[i][j]
		3	398	57.7	0.77	26.2[i][j]	150[i][j]
		Average	426	61.8	0.83	28.3	162
B	L-T	1	421	61.1	0.82	28.6[i][j]	163[i][j]
		2	421	61.1	0.82	25.2[i][j]	144[i][j]
		3	405	58.7	0.79	23.4[i][j]	134[i][j]
		Average	416	60.3	0.81	25.7	147
Properties from Unpublished Alcoa Data[p]	L-T		356	51.6	0.68	20.1	115
A	T-L	1	271	39.3	0.52	8.7[k][j]	50[k][j]
		2	281	40.8	0.54	23.3[k][j]	133[k][j]
		3	267	38.7	0.51	18.8[k][j]	107[k][j]
		Average	273	39.6	0.53	16.9	97
B	T-L	1	250	36.3	0.48	0.0[l][m]	0[l][m]
		2	266	38.6	0.51	0.0[l][m]	0[l][m]
		3	259	37.6	0.50	17.6[n][m]	100[n][m]
		Average	258	37.4	0.49	(o)	(o)
Properties from Unpublished Alcoa Data[p]	T-L		253	36.7	0.48	8.8	50

NOTES:
(a) Fabricated from a single lot.
(b) Sample No. 523713 (Alcoa number).
(c) Specimens taken from Section 2 in each piece (refer to Fig. 1 for location of Section 2).
(d) Refer to Figs. 3 and 4 for location of test specimens in pieces A and B, respectively.
(e) Test specimens taken in the longitudinal (L-T) and long-transverse (T-L) direction of rolling and from the center (T/2) location through the plate thickness.
(f) TS = Tear Strength.
(g) TS/YS = Tear Strength divided by Tensile Yield Strength.
(h) UPE = Unit Propagation Energy.
(i) UPE may be estimated and slightly high (rapid and diagonal fracture).
(j) Value included in the determination of average value.
(k) UPE may be estimated (rapid fracture).
(l) Energy may be near zero (curve not reliable).
(m) Value not included in the determination of an average value.
(n) UPE is estimated (rapid fracture).
(o) Not determined.
(p) Properties represent the results of tests of one (1) commercially produced sample of 34.9 mm (1.375-in.) thick 2020-T651 plate (one test in each orientation).

TABLE 4

RESULTS OF FRACTURE TOUGHNESS TESTS (PLANE-STRAIN (K_{Ic}), SLOW-BEND CHARPY (K_{Ich})) AT ROOM TEMPERATURE OF TWO (2) PIECES[a] OF COMMERCIALLY PRODUCED 32.54 mm (1.281-in.) THICK ALUMINUM ALLOY 2020-T651 PLATE[b]

Plate Piece[c][d] Identification	Specimen Orientation[e]	Specimen No.	K_{Ic} Tests: K_Q MPa$\sqrt{m}$	K_Q KSI$\sqrt{in.}$	Valid K_{Ic}[j]	Meaningful K_{Ic}[j]	Slow-Bend Charpy Tests: Specimen No.	K_{Ich} MPa$\sqrt{m}$	K_{Ich} KSI$\sqrt{in.}$
A	L-T	1	23.6	21.5	Yes	—			
		2	23.5	21.4	Yes	—			
		Average	23.6	21.5	Yes	—			
B	L-T	1	23.5	21.4	Yes	—	1[k]	20.2	18.4
		2	23.6	21.5	Yes	—	2[k]	20.9	19.0
		Average	23.6	21.5	Yes	—	Average	20.6	18.7
							3[l]	22.4	20.4
							4[l]	23.7	21.6
							Average	23.0	21.0
Properties from Unpublished Alcoa Data(1)	L-T		23.7[1]	21.6[1]	—	—			
A	T-L	1	19.2	17.5	No[f]	Yes[f]			
		2	19.0	17.3	No[f]	Yes[f]			
		Average	19.1	17.4	No	Yes			
B	T-L	1	18.8[g]	17.1[g]	No[f]	No[f]	1[k]	15.6	14.2
		2	18.6	16.9	No[f]	Yes[f]	2[k]	15.9	14.1
		Average	18.6[h]	16.9[h]	No	Yes	Average	15.6	14.2
							3[l]	16.3	14.8
							4[l]	16.8	15.3
							Average	16.6	15.0
Properties from Unpublished Alcoa Data(1)	T-L		19.1[1]	17.4[1]	Yes	—			

NOTES:
(a) Fabricated from a single lot.
(b) Sample No. 523713 (Alcoa number).
(c) Specimens taken from Section 2 in each piece (refer to Fig. 1 for location of Section 2).
(d) Refer to Figs. 3 and 4 for location of test specimens in pieces A and B, respectively.
(e) Test specimens taken in the longitudinal (L-T) and long-transverse (T-L) direction of rolling and from the center (T/2) location through the plate thickness.
(f) Test is invalid due to the Kf being greater than 0.60 K_Q for the last step of fatigue cracking (meaningful range is up to 0.70 K_Q).
(g) Value not included in the determination of average value.
(h) Value represents the result of one (1) test.
(i) Properties represent the results of tests of two (2) commercially produced samples of 34.9 mm (1.375-in.) thick 2020-T651 plate (a total of 4 tests in each orientation).
(j) Per ASTM Method E399.
(k) Specimen 10 mm (0.395-in.) in thickness.
(l) Specimen 6.35 mm (0.250-in.) in thickness.

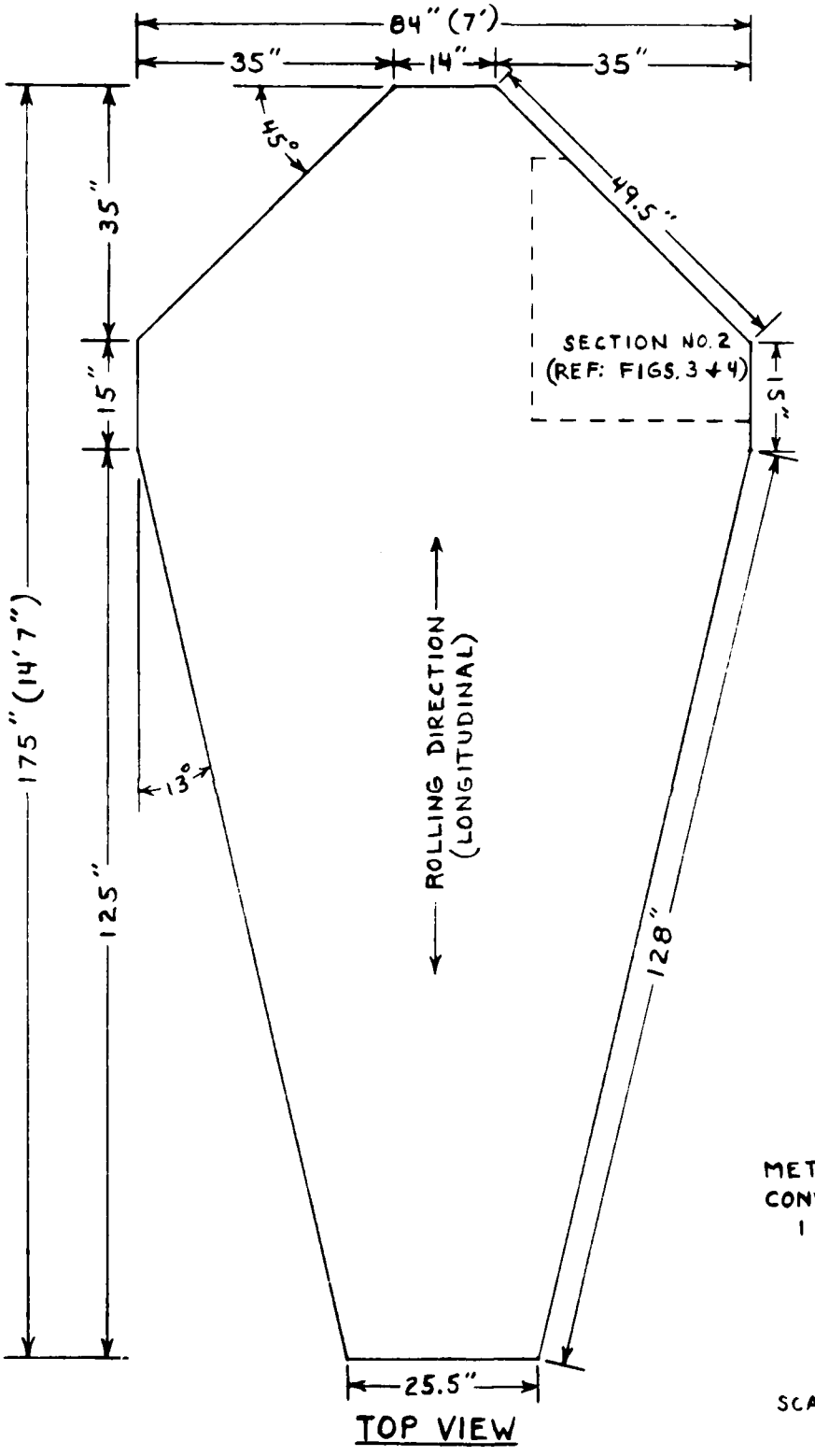

FIG. 1 SIZE AND SHAPE OF TWO PIECES OF COMMERCIALLY PRODUCED ALLOY 2020-T651 PLATE (1.281 IN. THICK) — SAMPLE S23713 (A+B)

METRIC (SI)
CONVERSION FACTOR:
1 IN. = 25.4 mm

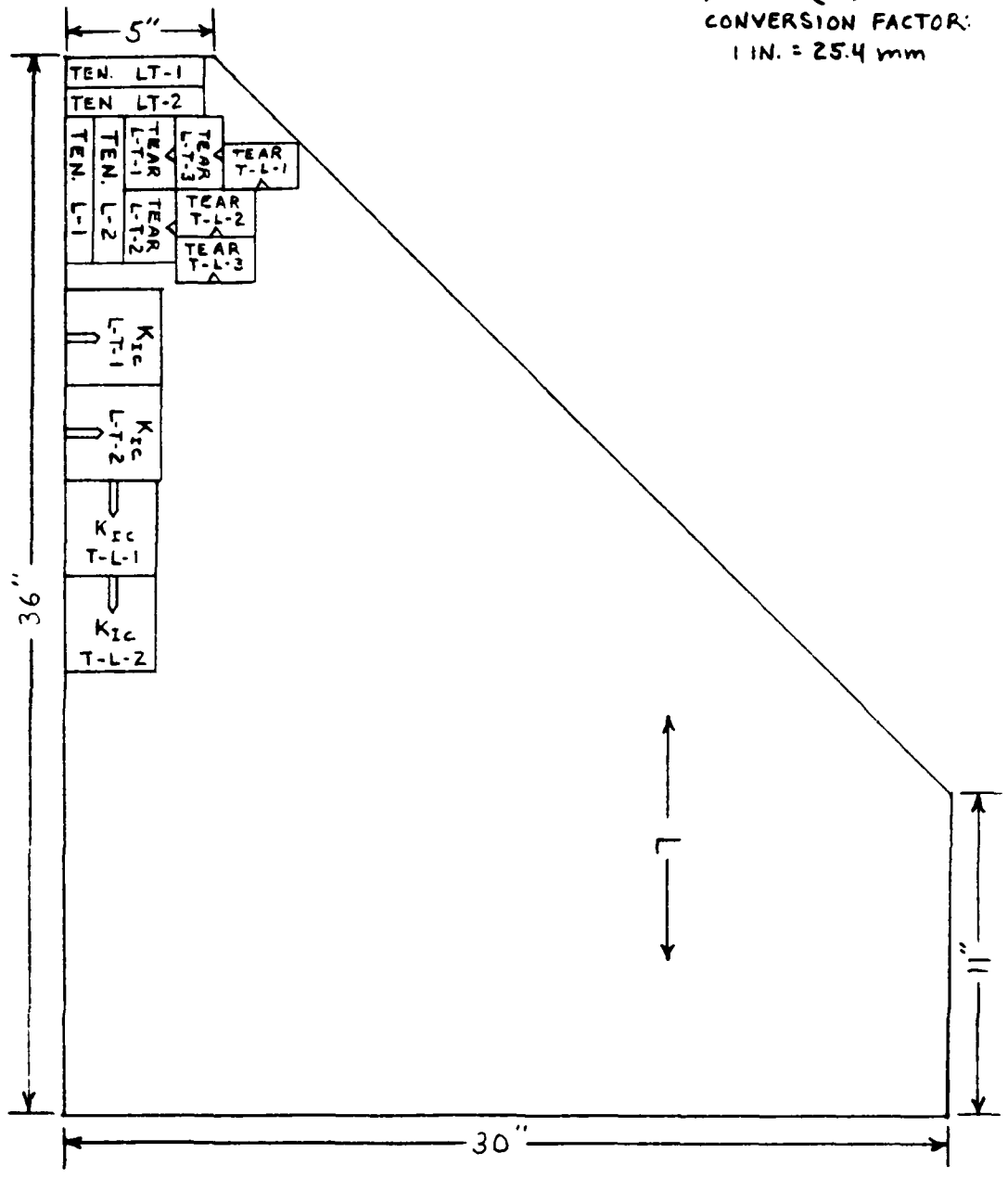

TOP VIEW

SCALE: 1 IN. = 5 IN.

FIG. 3 LOCATION OF TEST SPECIMENS, ALUMINUM ALLOY 2020-T651 PLATE (SAMPLE 523713, PIECE A, SECTION 2)

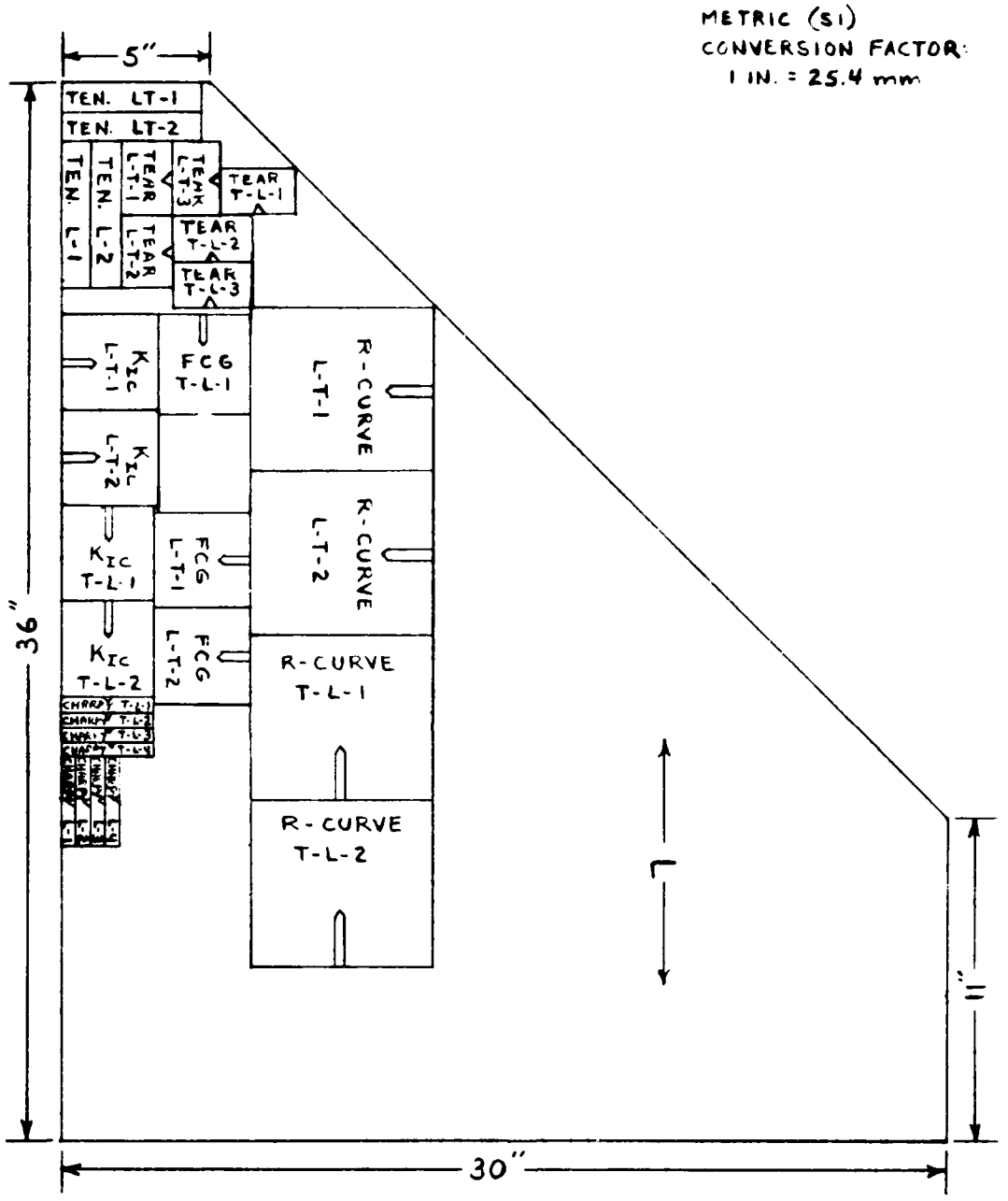

TOP VIEW

SCALE: 1 IN. = 5 IN.

FIG.4 LOCATION OF TEST SPECIMENS, ALUMINUM ALLOY 2020-T651 PLATE (SAMPLE S23713, PIECE B, SECTION 2)

Tear strength, psi = $\frac{P}{A} + \frac{MC}{I} = \frac{P}{bt} + \frac{3P}{bt} = \frac{4P}{bt}$

Unit propagation energy, in.-lb per sq in. = $\frac{\text{energy to propagate a crack}}{bt}$

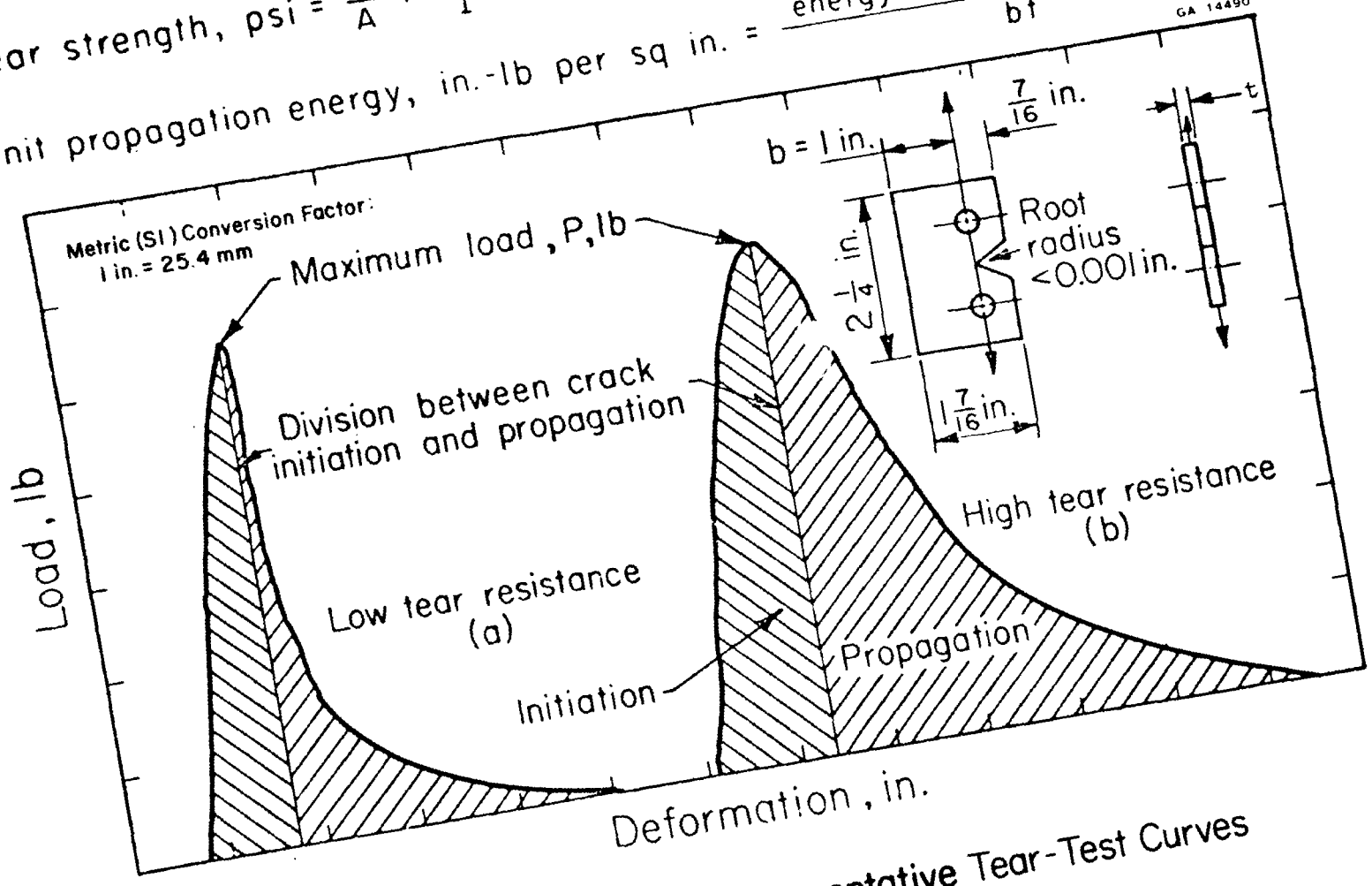

Tear-Test Specimen and Representative Tear-Test Curves
Figure 5

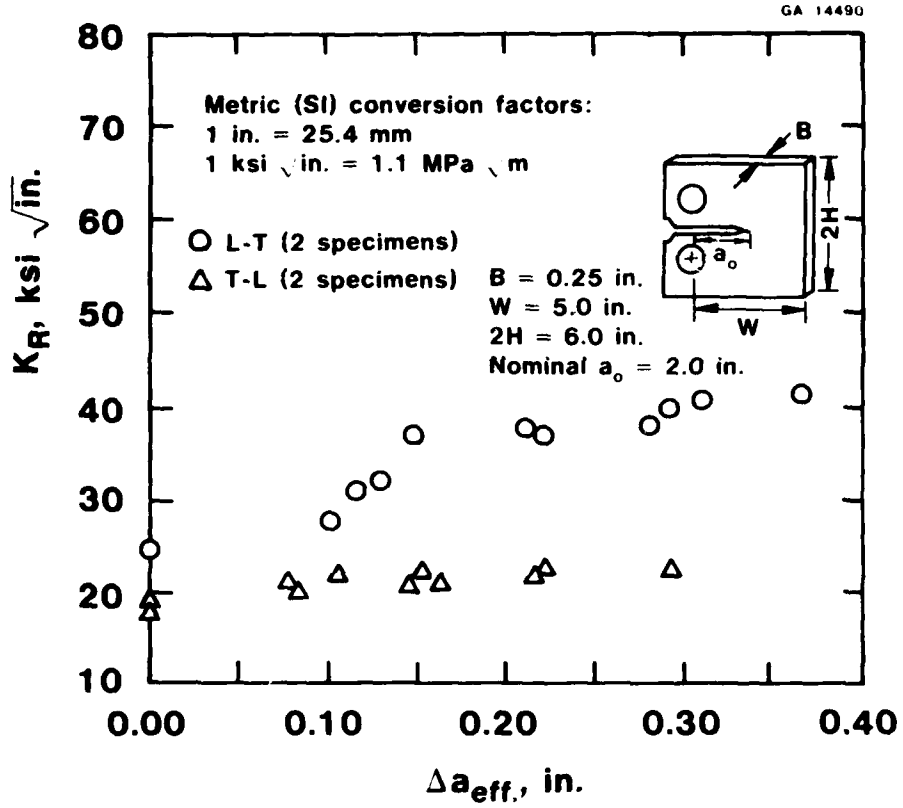

R-Curve Toughness Data for Commercially Produced 2020-T651 Plate (32.54 mm Thick) in the Longitudinal (L-T) and Long-Transverse (T-L) Orientations

Figure 6

GA 14490

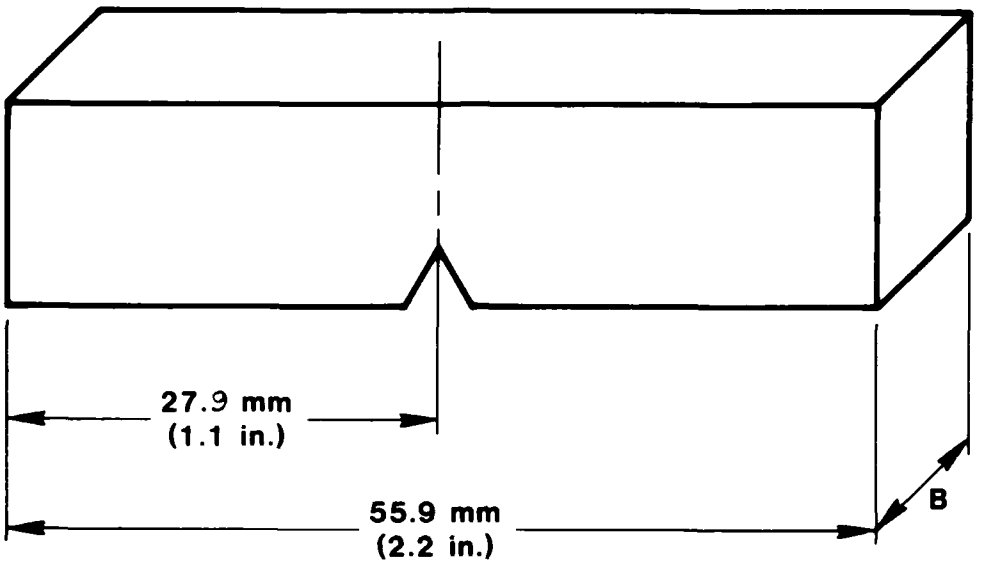

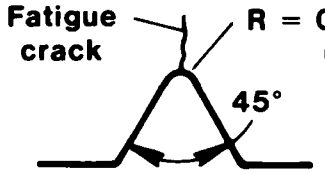

Enlarge view of notch

B = 6.35 ± 10 mm
(0.25 ± 0.395 in.)

Slow-Bend Charpy Specimen
Figure 7

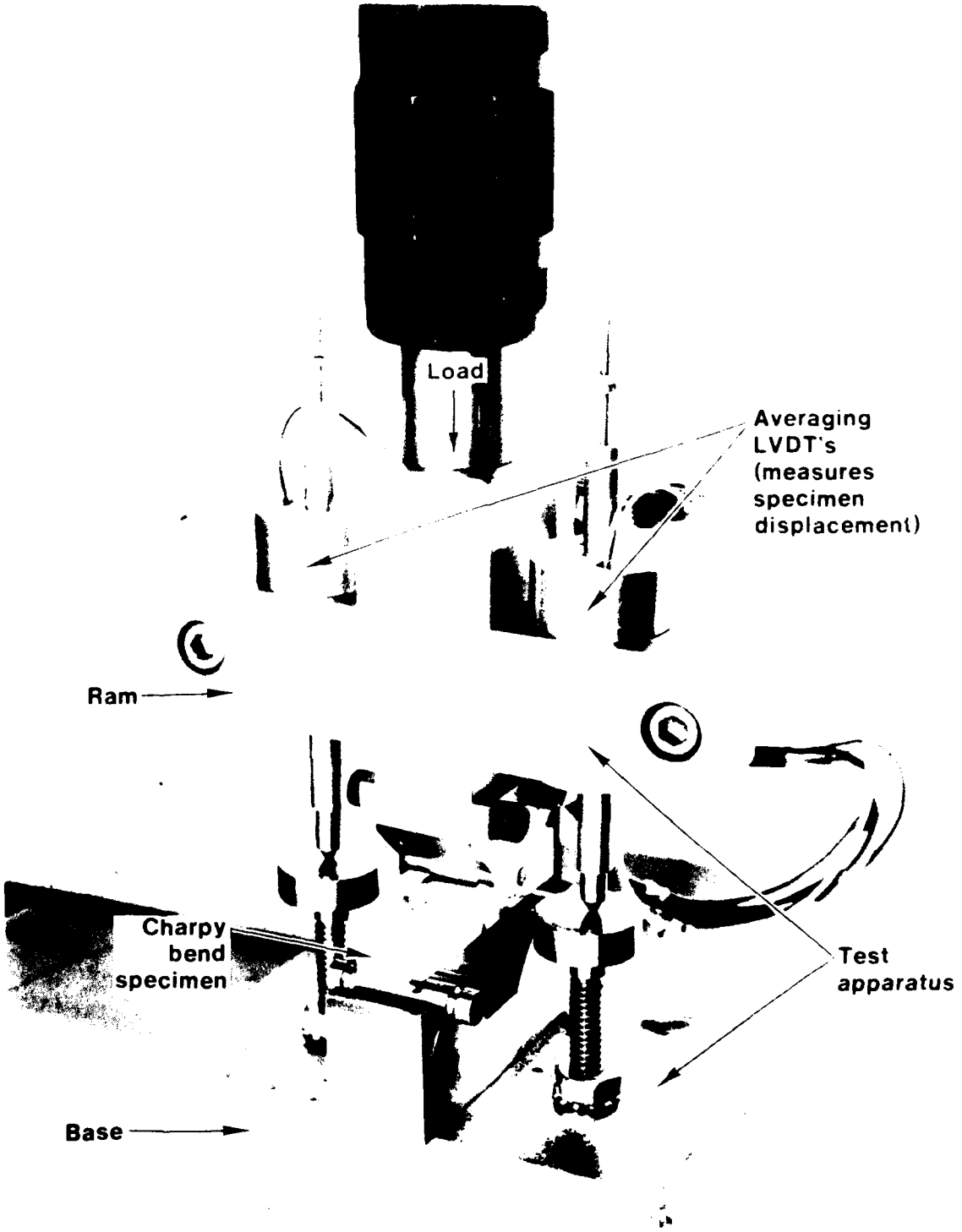

Slow-Bend Charpy Test Set-Up

Figure 8

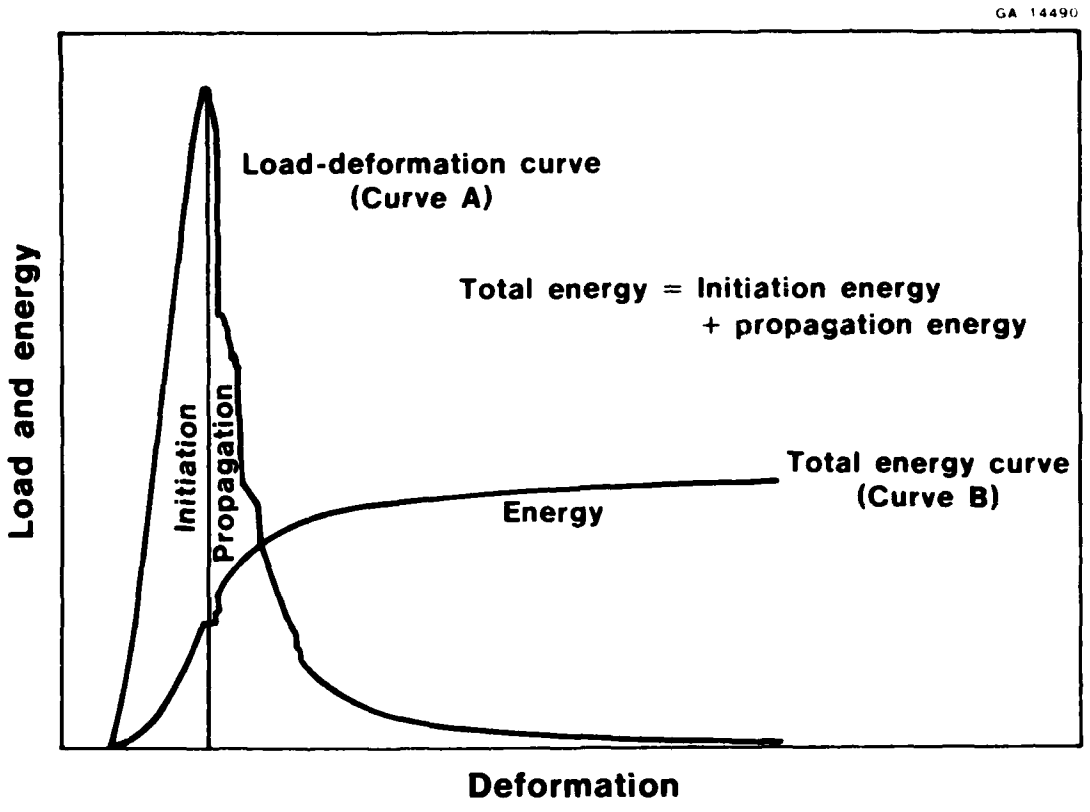

Representative Test Curve for Computer Logged Slow-Bend Charpy Test

Figure 9

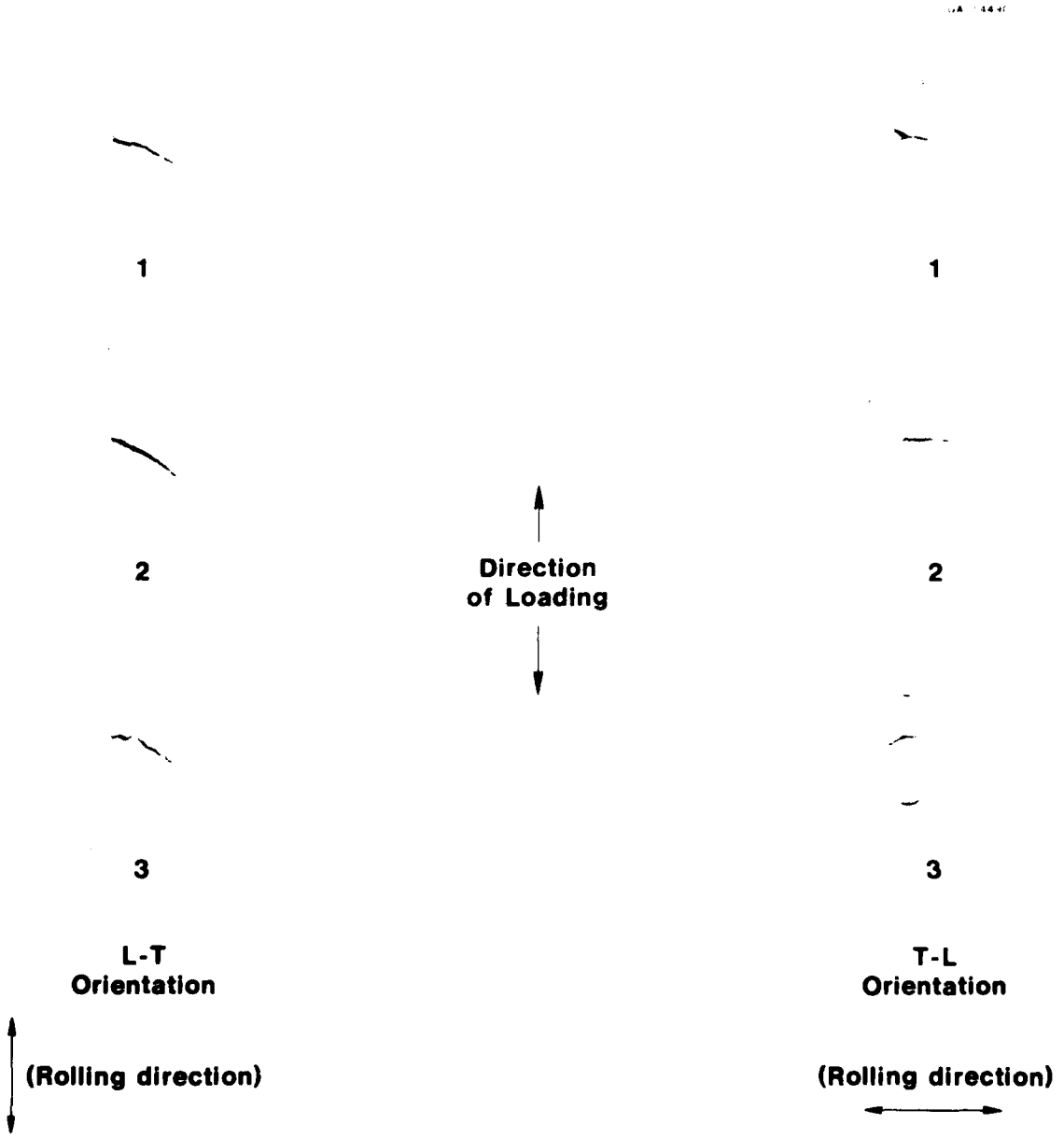

Effect of Specimen Orientation on the Fracture Path of Triplicate Kahn-Type Tear Specimens from a Sample (523713-A-2) of 2020-T651 Aluminum Alloy Plate (32.54 mm Thick)

Figure 10

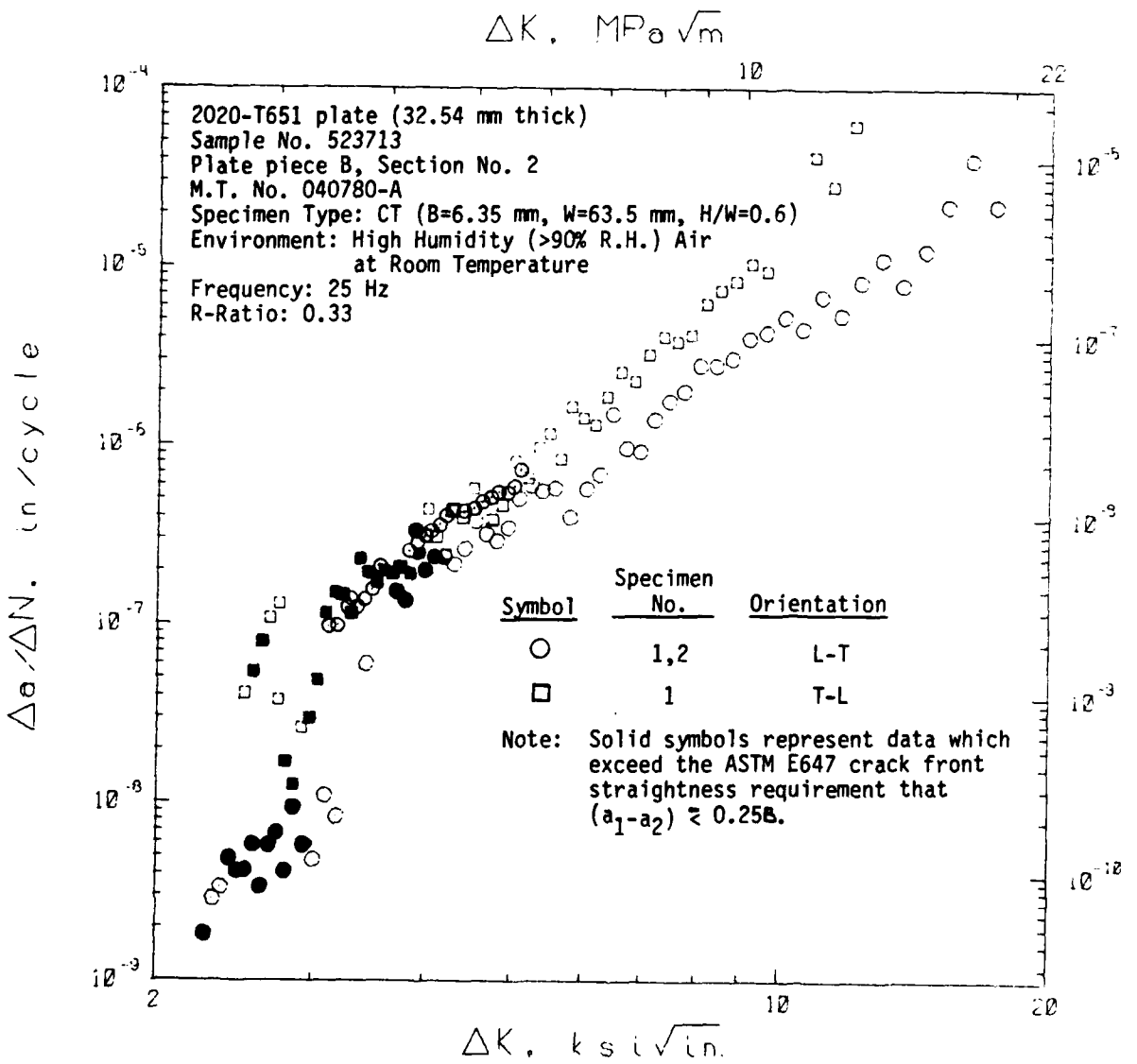

Fig. 11 Constant-Amplitude Fatigue Crack Propagation Data for Commercially Produced 2020-T651 Plate (32.54 mm thick) in the Longitudinal (L-T) and Long-Transverse (T-L) Orientations.
(Moist Air Environment, R-Ratio=0.33)

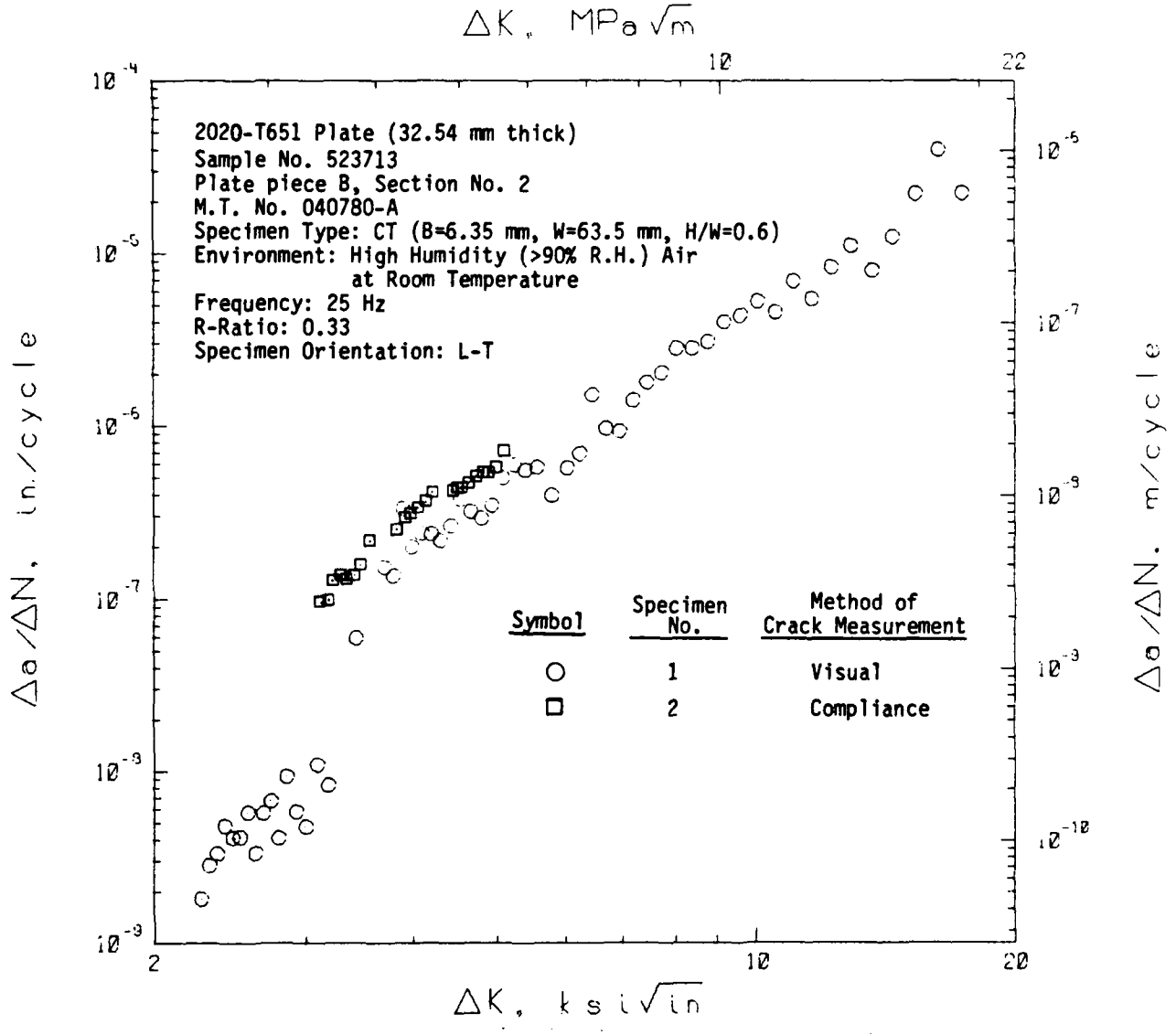

Fig. 12 Comparison of Constant-Amplitude Fatigue Crack Growth Rate Data Determined Using Visual Versus Compliance Methods of Crack Growth Measurement for Commercially Produced 2020-T651 Plate (32.54 mm thick) in the Longitudinal (L-T) Orientation

(Moist Air Environment, R-Ratio=0.33)

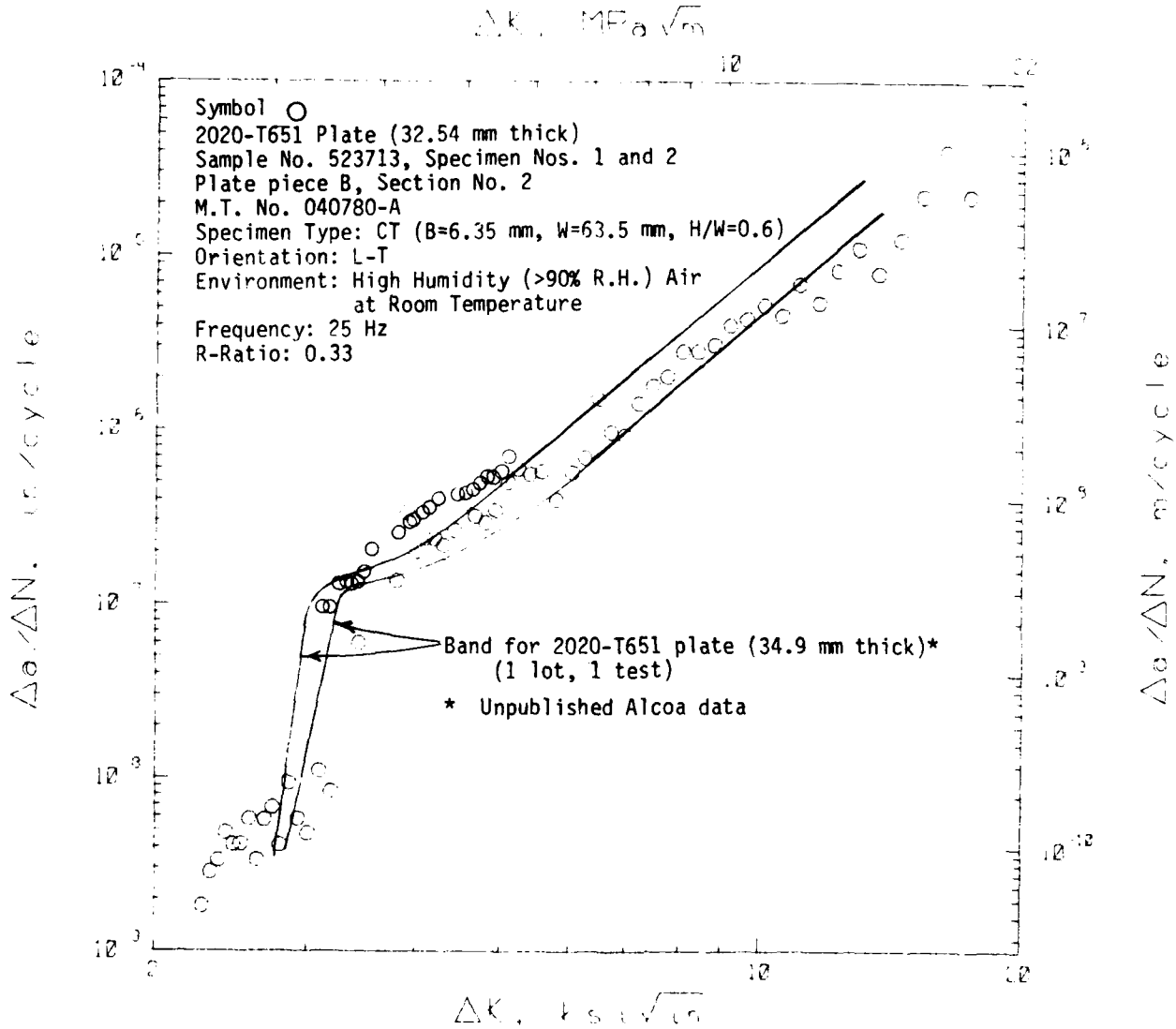

Fig. 13 Comparison of the Constant-Amplitude Fatigue Crack Propagation Data for Samples of Commercially Produced 2020-T651 Plate.
(Moist Air Environment, R-Ratio=0.33, L-T Orientation)

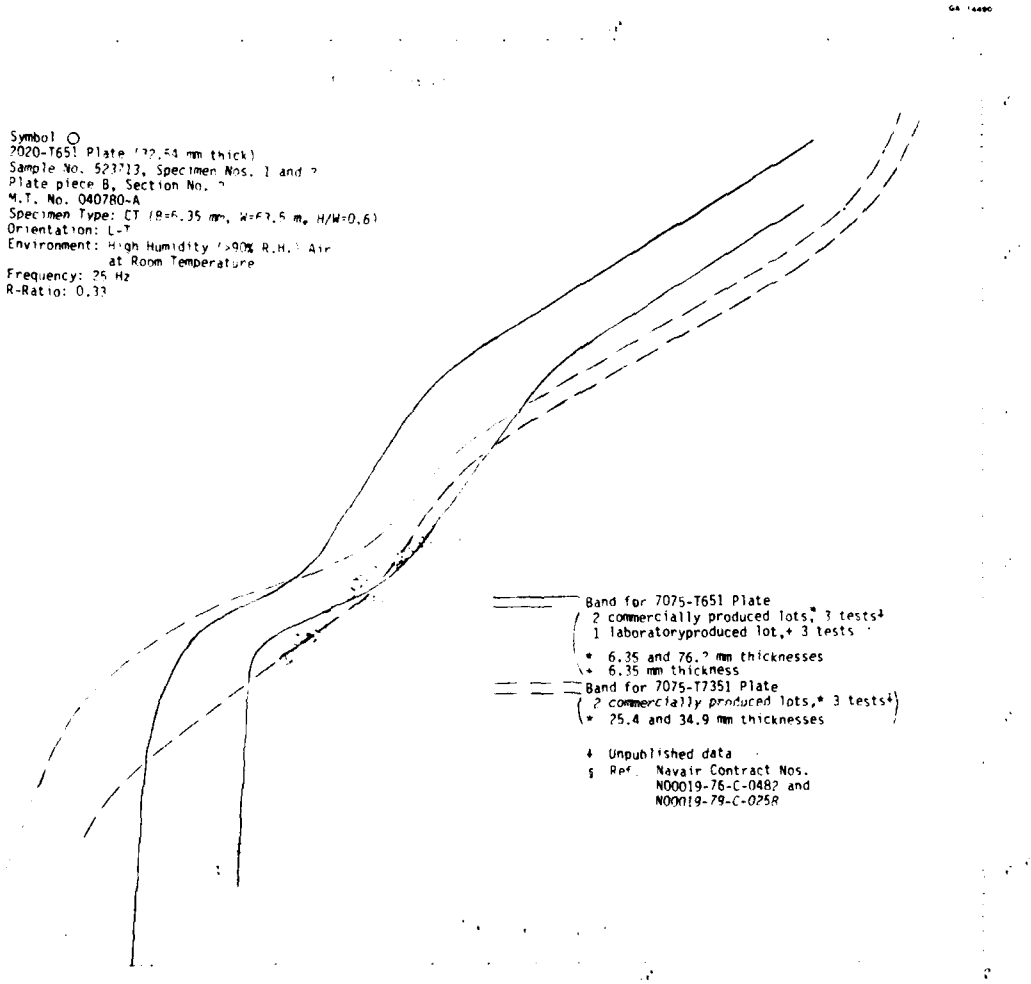

Fig. 14 Comparison of Constant-Load-Amplitude Fatigue Crack Propagation Data for Commercially Produced 2020-T651 Plate with Data for Commercially and Laboratory Produced 7075-T651 Plate and Commercially Produced 7075-T7351 Plate
(Moist Air Environment, R-Ratio=0.33, L-T Orientation)

(a)
da dN = 1.27 · 10 ^{10} m cycle
(5 · 10 ^{9} in. cycle)

Propagation direction

(b)
da/dN = 2.54 · 10^{-10} m/cycle
(1 · 10^{-8} in./cycle)

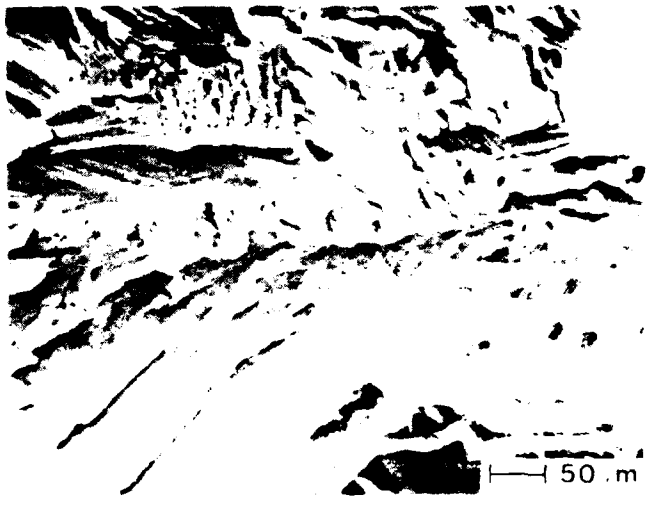

Fracture Surface Appearance of Alloy 2020-T651 Plate (32.54 mm Thick) in the L-T Orientation for FCG Rates (da/dN) of 1.27 × 10^{-10} and 2.54 × 10^{-10} m/cycle (5 × 10^{-9} and 1 × 10^{-8} in./cycle, respectively)

Figure 15 (a and b)

(c)
$da/dN = 1.27 \times 10^{-9}$ m/cycle
$(5 \times 10^{-8}$ in./cycle)

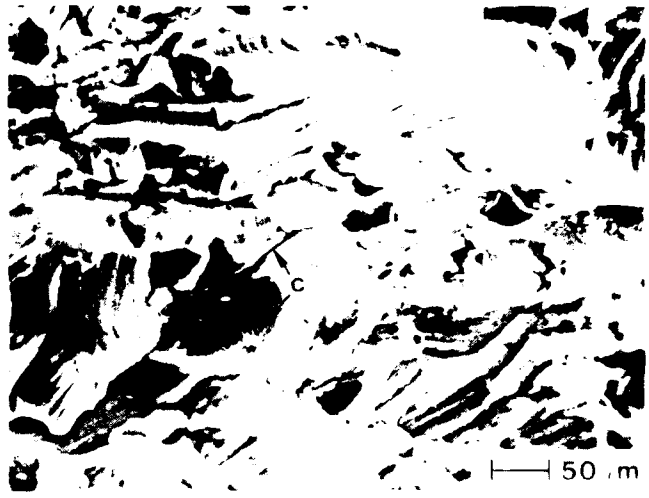

Propagation direction

(d)
$da/dN = 1.27 \times 10^{-8}$ m/cycle
$(5 \times 10^{-7}$ in./cycle)

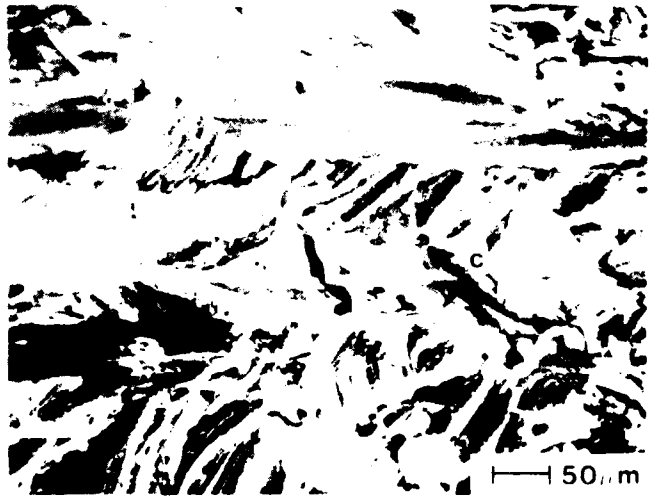

Fracture Surface Appearance of Alloy 2020-T651 Plate (32.54 mm Thick) in the L-T Orientation for FCG Rates (da/dN) of 1.27×10^{-9} and 1.27×10^{-8} m/cycle (5×10^{-8} and 5×10^{-7} in./cycle, respectively)

Figure 15 (c and d)

(e)
da dN 1.27 10 7 m cycle
(5 10 6 in. cycle)

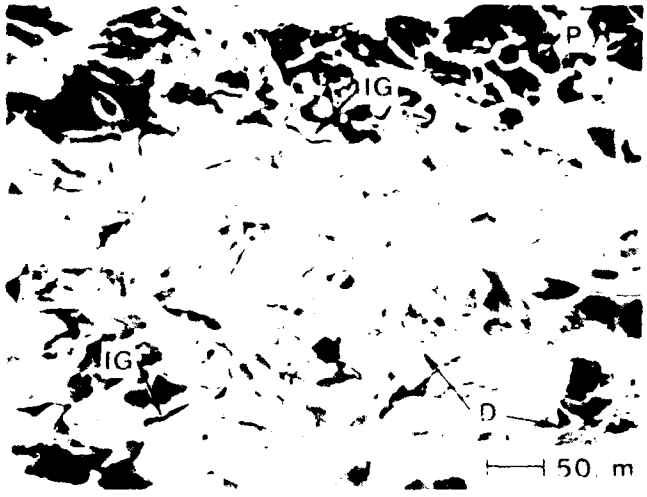

Propagation direction

(f)
da/dN = 1.27 · 10^{-6} m/cycle
(5 · 10^{-5} in./cycle)

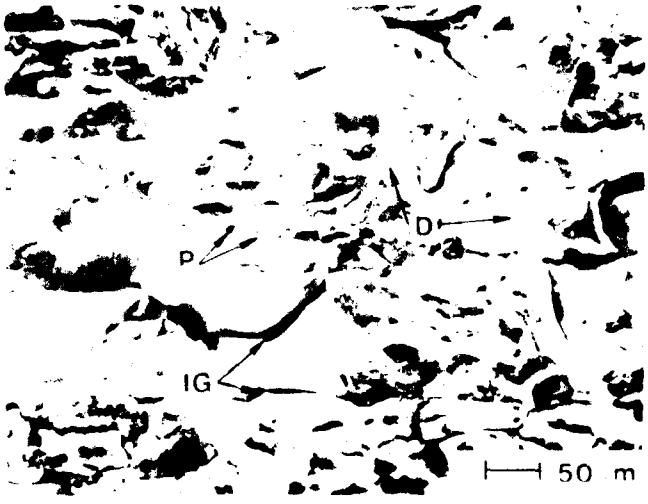

Fracture Surface Appearance of Alloy 2020-T651 Plate (32.54 mm Thick) in the L-T Orientation for FCG Rates (da/dN) of 1.27 × 10^{-7} and 1.27 × 10^{-6} m/cycle (5 × 10^{-6} and 5 × 10^{-5} in./cycle, respectively)

Figure 15 (e and f)


DATE
FILMED
7-8